

RESEARCH ARTICLE

10.1029/2019JC015421

Key Points:

- Atmospheric conditions can have substantial impacts on coastal sea levels beyond extreme events
- Classifications of patterns of several atmospheric variables can be used to reconstruct a time series of anomalous sea level

Supporting Information:

- Supporting Information S1
- Figure S1
- Figure S2
- Figure S3
- Figure S4
- Figure S5
- Figure S6
- Figure S7
- Figure S8

Correspondence to:

S. C. Sheridan,
sshrid1@kent.edu

Citation:

Sheridan, S. C., Lee, C. C., Adams, R., Smith, E. T., Pirhalla, D., & Ransibrahmanakul, V. (2019). Temporal modeling of anomalous coastal sea level values using synoptic climatological patterns. *Journal of Geophysical Research: Oceans*, 124, 6531–6544. <https://doi.org/10.1029/2019JC015421>

Received 26 JUN 2019


Accepted 22 AUG 2019

Accepted article online 29 AUG 2019

Published online 4 SEP 2019

©2019. American Geophysical Union.
All Rights Reserved.

Temporal Modeling of Anomalous Coastal Sea Level Values Using Synoptic Climatological Patterns

Scott C. Sheridan¹ , Cameron C. Lee¹, Ryan E. Adams¹, Erik T. Smith¹, Douglas E. Pirhalla², and Varis Ransibrahmanakul²

¹Department of Geography, Kent State University, Kent, OH, USA, ²National Center for Coastal Ocean Science, NOAA, Silver Spring, MD, USA

Abstract Short-term changes in sea level can have substantial impacts on coastlines, and increases in coastal flooding have been observed as the mean sea level continues to climb. While extreme events such as hurricanes have been well studied in terms of their impacts on anomalous sea level values, anomalous sea levels due to less extreme atmospheric events have been less well studied, despite the increases in nuisance flood events that have occurred. In this study, we assess the relationship between short-term atmospheric circulation patterns and anomalous coastal sea level values for all oceanic tidal gauges in the conterminous United States for the period 1979–2016. Atmospheric patterns are depicted using self-organizing maps for four variables: sea level pressure, 10-m wind, 850-mb temperature, and 700-mb geopotential height. We then reconstruct the time series of anomalous sea level through nonlinear autoregressive models with exogenous input (NARX models), an artificial neural network-based time series model. Results show that these four atmospheric variables can successfully model sea level, with a correlation between model and observation using a closed-loop (open-loop) architecture of 0.83 (0.64), with a median absolute error of 3.34 (4.90) cm. The model generally performs better in winter than summer, and along the Pacific Coast than the Atlantic and Gulf Coasts. By using the NARX methodology, we intend to next assess its utility as a forecasting tool.

Plain Language Summary Coastal flooding is becoming an increasing concern as sea level continues to rise. Beyond extreme events, there are many “blue sky floods” in which atmospheric conditions synergize to produce high sea levels. In this paper, we examined how well we could simulate the time series of anomalous sea level values along the U.S. coast using atmospheric conditions. Our results show significant potential in replicating sea level values. We next plan to evaluate how well our model can be used in a forecasting capacity.

1. Introduction

Within the context of the secular trend of rising global mean sea level (e.g., Church & White, 2011), there are numerous deviations of coastal sea levels on varied spatial and temporal scales. Temporal trends at any given location are strongly affected by vertical land movement (Wöppelmann & Marcos, 2016). El Niño–Southern Oscillation can influence global mean sea level as well as regional variability (Cazenave et al., 2014; Hamlington et al., 2015; Jevrejeva et al., 2003). Beyond global phenomena, seasonal to interannual sea level variability depends on myriad factors, one of which is wind forcing (Piecuch & Ponte, 2011). For instance, while seasonal anomalies may depend upon variability in ocean circulation, such as the Atlantic Meridional Overturning Current, the strongly negative North American Oscillation may have played a substantial role in persistently high sea levels along the northeastern U.S. coast in 2009–2010 (Goddard et al., 2015). Further, seasonal sea level anomalies have also been associated with the North American Oscillation in the Mediterranean Sea (Landerer & Volkov, 2013) and the Arctic Oscillation in the North Atlantic (Jevrejeva et al., 2003).

On shorter time scales, the most damaging increases in sea levels along coasts typically occur with storm surges associated with tropical cyclones, such as the \$70 billion in damage done by Hurricane/Cyclone Sandy in 2012 (National Oceanic and Atmospheric Administration, 2013). Beyond these well-studied catastrophic events, for many analyses of ocean-atmospheric interactions, multiple atmospheric forces can play a role, including atmospheric pressure, circulation, wind stress, storm surges, and wind-induced Ekman transport (Sheridan et al., 2017; Sweet et al., 2009). The role of short-term atmospheric influences on sea levels has typically focused on the role of atmospheric pressure as the “inverted barometer” effect

(Wunsch & Stammer, 1997), and the role of atmospheric wind fields has been assessed as well in terms of modeling (Carrere & Lyard, 2003). Frequency of storminess can be related to changes in sea level as well (Thompson et al., 2013). Longitudinal studies of the atmospheric causal mechanisms behind anomalous coastal sea levels are sparse and have pointed to multiple different mechanisms, such as Cassano et al. (2006) who show wind duration to be more important than wind direction for flooding at Barrow, Alaska, or Colle et al. (2010), who show storm tracks, as well as fetch, play a role in New York City floods.

One method of analyzing the holistic influence of the atmosphere is through the use of synoptic climatology, more specifically, through atmospheric circulation pattern identification (Lee & Sheridan, 2015). Each discrete atmospheric pattern (AP) over a region can then be related to an expected set of surface conditions, and their occurrence could be associated with anomalous marine events. There are two known studies that have used synoptic patterns to assess anomalous sea levels: Neal et al. (2018) used sea level pressure (SLP) patterns derived by the U.K. Met Office to estimate likelihood of coastal flooding along the coast of the United Kingdom and our previous study (Sheridan et al., 2017), discussed further below.

Though there have been numerous different methodologies to classify APs, in recent years, one method of classification has become increasingly used: self-organizing maps (SOMs; Sheridan & Lee, 2011), an artificial neural network (ANN)-based classification technique in which circulation patterns are ordered in a two-dimensional continuum of patterns, with more similar patterns located in closer proximity than more dissimilar patterns. SOMs have been shown to be effective at examining the association between atmospheric circulation on coastal sea levels in our previous work for the mid-Atlantic Coast of the United States (Sheridan et al., 2017).

The synoptic methodology has some limitations; for instance, it will not fully capture the most extreme atmospheric events (e.g., hurricanes), due to their atmospheric circulations being effectively “unique” and thus hard to generalize. However, the categorization of the atmosphere into patterns yields substantive statistical power to assess the correlation between the atmosphere and ocean properties. Further, the synoptic methodology serves as an effective statistical downscaling tool for output from weather forecasting or global climate models (Schoof, 2013) and in cases has proven to be superior to finer-scale model-generated atmospheric data (Wetterhall et al., 2009). This ability makes it especially useful for midrange forecasting, where models would be unable to render atmospheric features with sufficient precision for dynamic modeling. One such approach for midrange forecasting is the use of nonlinear autoregressive models with exogenous input (NARX models), which are ANN-based time series models that can account for complex, temporally auto-correlated variables; we have already used NARX models in a similar context to simulate water clarity along the Gulf Coast of the United States (Lee et al., 2017).

In this research, we extend the work presented in Sheridan et al. (2017), to assess the relationship between short-term to seasonal-term atmospheric circulation patterns and anomalous coastal sea level values for all oceanic tidal gauges in the conterminous United States for the period 1979–2016. We present this work using the NARX methodology to simulate the time series of anomalous sea level for future evaluation as a forecasting tool.

2. Materials and Methods

2.1. Anomalous Sea Level Values

The coastal sea level data used in this research are mean observed and predicted daily tidal gauge data available from the National Oceanic and Atmospheric Administration CO-OPS for the conterminous United States. All stations for which at least 50% of data are available for the period 1979–2016 are used, including 42 along the Atlantic Ocean, 20 along the Gulf of Mexico, and 28 along the Pacific Coast. The predicted data are subtracted from the observed data to eliminate the astronomical component of sea level variability, to create “residual” sea level values. Since predicted tidal gauge data do not include seasonality other than astronomical forcing, or secular trends, data needed to be further standardized. Secular trends were removed using a third- or fourth-order polynomial that was fit across the full time series, with the order of polynomial being the lowest order beyond which the fit did not statistically significantly improve. Seasonal variability was removed by subtracting the remaining monthly mean anomaly (averaged across all years) from the data once secular trends were removed. These two processes yielded the final anomalous sea level values.

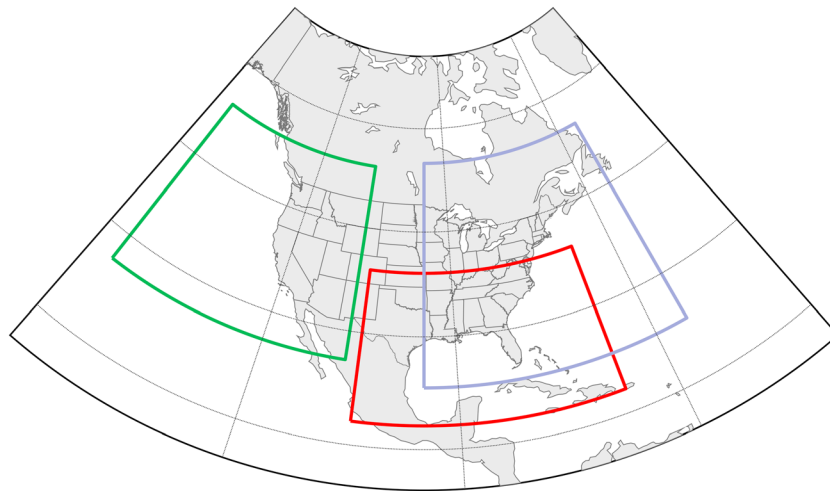


Figure 1. The three domains used in the classification of atmospheric data into self-organizing map-based classifications: Atlantic (purple), Gulf (red), and Pacific (Green).

In order to provide a more robust assessment on coastal sea level variability and to create complete time series, individual stations were then clustered into regions using a K-means cluster analysis. The cluster analysis was based on a principal components (PCs) analysis of individual station daily anomalous sea level time series z scores, and the resulting clusters grouped together stations with similar temporal variability.

2.2. Atmospheric Data and Circulation Patterns

To categorize atmospheric data into synoptic patterns, spatially cohesive, complete, and representative data are derived from the North American Regional Reanalysis (Mesinger et al., 2006) project. We selected four daily mean variables for analysis:

1. *SLP*, for its ability to capture the broad-scale circulation of the lower troposphere as well as the inverse barometric pressure effect; further, in our previous work (Sheridan et al., 2017) SLP was shown as an optimal predictor of sea level anomalies;
2. *near-surface (10-m) wind (WIND)*, to depict most clearly the near-surface wind stress of the atmosphere on the surface of the ocean;
3. *850-mb temperature (850T)*, a broad measure of lower-tropospheric temperatures that may be helpful in approximating the impact of sea surface temperatures (e.g., Pirhalla et al., 2015) on sea level height via thermal expansion; and
4. *700-mb geopotential heights (700Z)*, representative of midtropospheric circulation, and an important modulator of the impact of SLP on coastal flood likelihood from Sheridan et al. (2017).

Other atmospheric variables were considered from other prior work performed, most particularly Sheridan et al. (2017). Given the varied surfaces incorporated into each SOM domain, parameters too close to the ground (e.g., 2 m or surface) would be affected by boundary layer conditions, which the SOM would inappropriately hone in on at the expense of broader-scale patterns. Other upper atmospheric parameters, such as 500-mb geopotential heights, were also evaluated, with minimal difference from 700-mb heights.

AP classification can be impacted by the size and boundaries of the spatial domain in which they are classified (Beck et al., 2013). In a practical sense, the use of too large of a domain (e.g., continental scale) would likely yield poor relationships between patterns and sea levels, as variability over land (e.g., an anticyclone over the Great Plains) would unnecessarily influence the categorization; too small of a categorization may focus on microscale features and miss the broader atmospheric circulation. Thus, in this project we defined three subcontinental domains (Figure 1).

SOMs have been shown to be generally the most stable and replicable of all synoptic classifications (Philipp et al., 2014), and based on this as well as their success in our previous work examining sea level variability (Sheridan et al., 2017), we used SOMs in this research. SOMs are an ANN-based, unsupervised clustering

technique that allows for an easy visualization of a clustering solution (Sheridan & Lee, 2011). SOMs are initialized using a uniform two-dimensional rectangular grid, with a user-defined number of nodes placed at the intersections of these grid lines, spanning the data space of the two leading PCs of the data set. The SOM neural network is trained in an iterative manner, whereby during each iteration, each observation (e.g., a daily field of SLP) is assigned to the node that it is most nearby in the data space (termed the best matching node). The position of this best matching node is adjusted slightly, moving a certain distance (which is defined using a “learning rate” parameter) toward the observation assigned to it. Nearby nodes within a certain “neighborhood distance” are also moved toward the observation, but to a lesser extent, while maintaining their order in the overlying grid. These adjustments continue until a user-defined number of iterations through the data set are completed, with the learning rate and neighborhood distance decreasing at each iteration.

The resulting grid morphs during training to eventually envelop the data and cluster more nodes into areas of more observations. Each node represents a separate AP that is situated on the SOM according to its similarity to the immediately adjacent nodes. Through these means, the SOM method promotes a more intuitive visualization of the classification as it naturally organizes the resultant patterns onto a two-dimensional plane with highly different APs typically in opposite corners, and more similar ones adjacent to each other. When complete, the SOM method ultimately categorizes each day into the node (AP) it most closely resembles.

Twelve separate SOMs were created, one for each of the three domains for each of the four variables: retained PCs (with eigenvalues > 1) scores of SLP, WIND, Z700, and T850. For each region, multiple classifications were completed to determine the optimal SOM dimension (e.g., a 5×4 SOM vs. a 7×5 SOM) necessary to capture regional-scale APs while still rendering smaller-scale processes critical to sea level variability. Ultimately, the appropriate number of APs (SOM nodes) is based on these nodes encompassing the full range of variability in the data, minimizing the within-node variability (cohesiveness) while maximizing the variability across nodes (separation; Hewitson & Crane, 2002; Yarnal, 1993). Two internal (with PC scores) and external (sea level data) cluster validation metrics—the Davies-Bouldin index (Davies & Bouldin, 1979) and the distributed variability skill score (Lee, 2017) were computed to determine the optimal SOM dimensions. Once classified, for each SOM the mean field of the variable for all days assigned into each node was calculated and mapped.

2.3. NARX Time Series Modeling

Next, the time series of sea level anomalies were simulated using NARX models, which are ANN-based time series models. NARX models are nonparametric, allowing for highly complex relationships between dependent and predictor variables to emerge, given adequate data (Diaconescu, 2008). Further, due to their autoregressive nature, NARX models naturally incorporate the temporal correlation of both the predictand (anomalous sea level) and the exogenous (AP) variables into modeling. The nonlinear relationships between weather and various oceanographic parameters and the autoregressive nature of a time series of sea level heights make NARX models ideal for this work; NARX models were also used successfully in modeling climate-water clarity relationships in Lee et al. (2017).

After clustering the tidal gauge stations into regions, separate NARX models were trained for each region using customized modeling scripts and the Neural Network Toolbox in Matlab (Beale et al., 2010). Prior to modeling, the proper exogenous variables were selected for each tidal gauge region. This input variable selection process was undertaken using principal components analysis and partial correlations between sea levels and multiple *potential* predictors, including the occurrence of each individual regional AP for each variable; the first five PCs of each variable for which a SOM was created, and seasonal and secular trends. For each variable, temporal lags were considered, with potential predictors including each value ranging from 0 to 14 days before the day of the anomalous sea level value it predicts. These potential predictors were subjected to principal components analysis, and only the 20 most highly correlated (in terms of absolute values of Spearman's rho) PCs were retained as the actual predictors for NARX modeling.

Implementation of NARX models generally requires only two user-defined parameters: the number of delays (lags) in the predictand and predictor variables and the number of neurons (complexity) to be included in the modeling framework. While greater complexity (neurons) would allow for a better trained

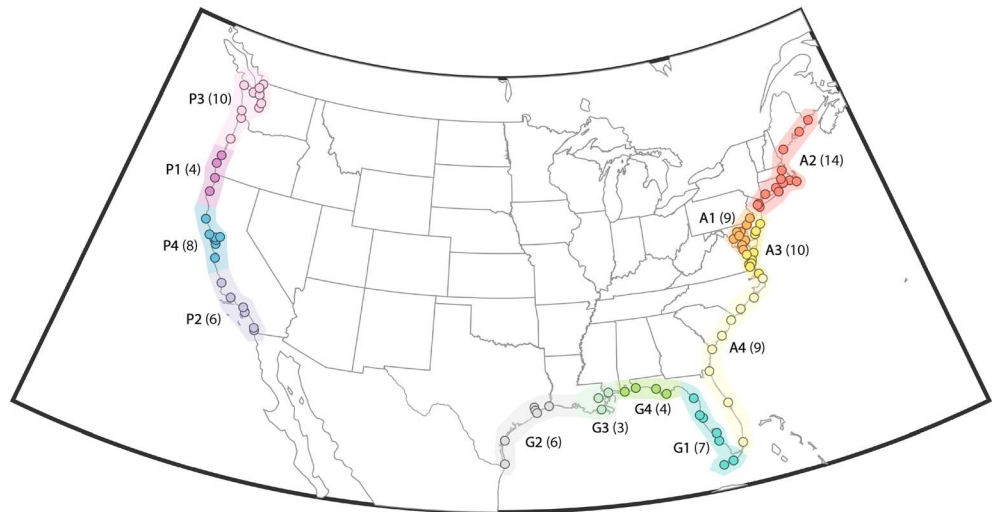


Figure 2. The 12 tidal gauge regions identified in the region; each circle within the region represents an individual station. The letter and number combination refer to the region name, and the number in parentheses is the number of stations within the region.

model, this also increases the chances of overfitting; likewise, the inclusion of nonsignificant time lags (in either the predictand or the predictors) would unnecessarily complicate the model and lead to the same issues. Thus, multiple combinations of neurons and delays were examined to see which combination yielded the best performing model in each region.

Model assessment was performed by first splitting the data into three contiguous timeblocks: training, internal validation, and independent testing. Training data were the largest block (60% of days) and are the data used by the ANN to “learn.” After each incremental change of weights and biases (a learning epoch) derived from the *training block* of data, the model is then simulated on *the internal validation block* of data, and the performance (mean square error) is measured. If the performance on this block of data fails to improve after a user-defined number (5) of consecutive learning epochs, then learning ceases, and the model trained five epochs ago is selected as optimal. Since this internal validation data set slightly influences the model, it cannot be considered completely independent, and thus, the third, *independent testing* block of data can be used for external validation of the model.

In Lee et al. (2017), multiple different partitions of the data into time blocks were evaluated and used in a block-jackknifing technique, whereby the model was trained multiple times using different time windows for the independent testing blocks of data and then chronologically reconstructing these outputs to get a complete time series estimate of model performance that could be considered independent from training. A similar approach was used in this research to gauge model performance for each tidal gauge region, using 10 different models. The error statistics discussed below were calculated from these independent reconstructed data sets to assess model performance against actual observed sea levels. Since each NARX model is initialized using random weights and biases, each of these models was also run in ensemble form, where 10 separate models were trained for each of the 10 testing block settings—resulting in the final output being an ensemble average of 100 models for each region.

NARX model complexity prevents a simple interpretation of the relative importance of each predictor variable in each NARX model. However, this relative importance can be estimated using a predictor-constant replacement method: Each model was rerun with a single predictor (the 20 PCs) set to a constant value (0) at all time steps, effectively removing it from the model. The change in the model’s performance (using median absolute error; MdAE) using this replacement was noted, and this process repeated for each predictor in each model. These changes in MdAE were then standardized, multiplied by the standardized loadings of the retained PCs for each variable, averaged across lag days, and turned into a percentage relative to all other variables. Comparative analyses of these changes in performance for all the included predictors in a

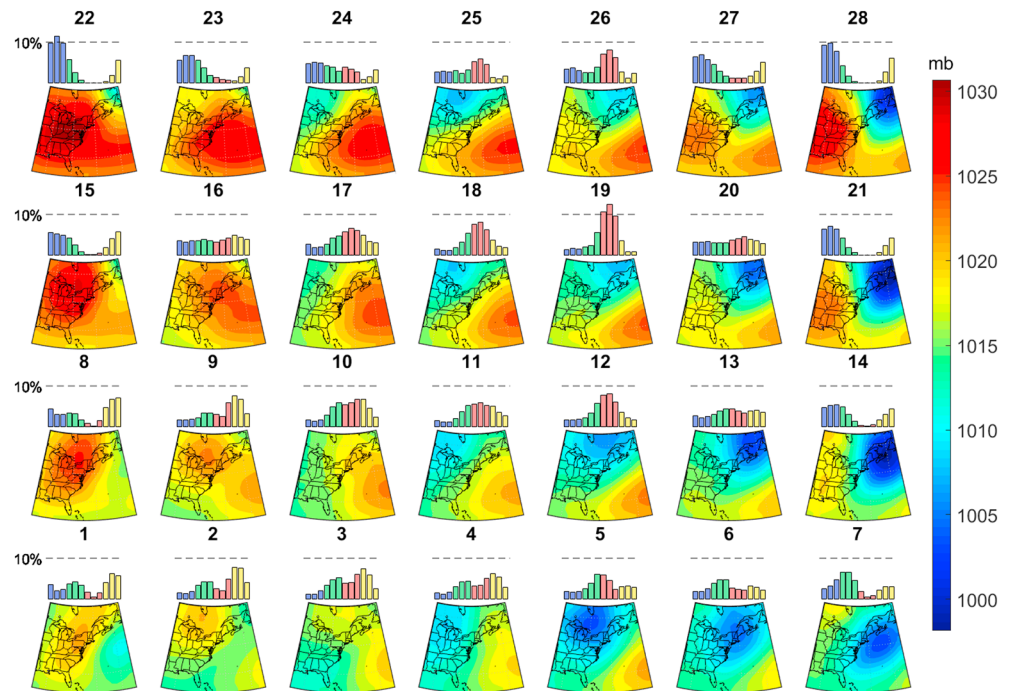


Figure 3. Self-organizing map for the Atlantic domain using sea level pressure. Maps are of mean fields of all days classified into each of the 28 nodes; the colored columns above each map represent the mean monthly frequency of that node over the period of study, December–February (blue), March–May (green), June–August (red), and September–November (yellow).

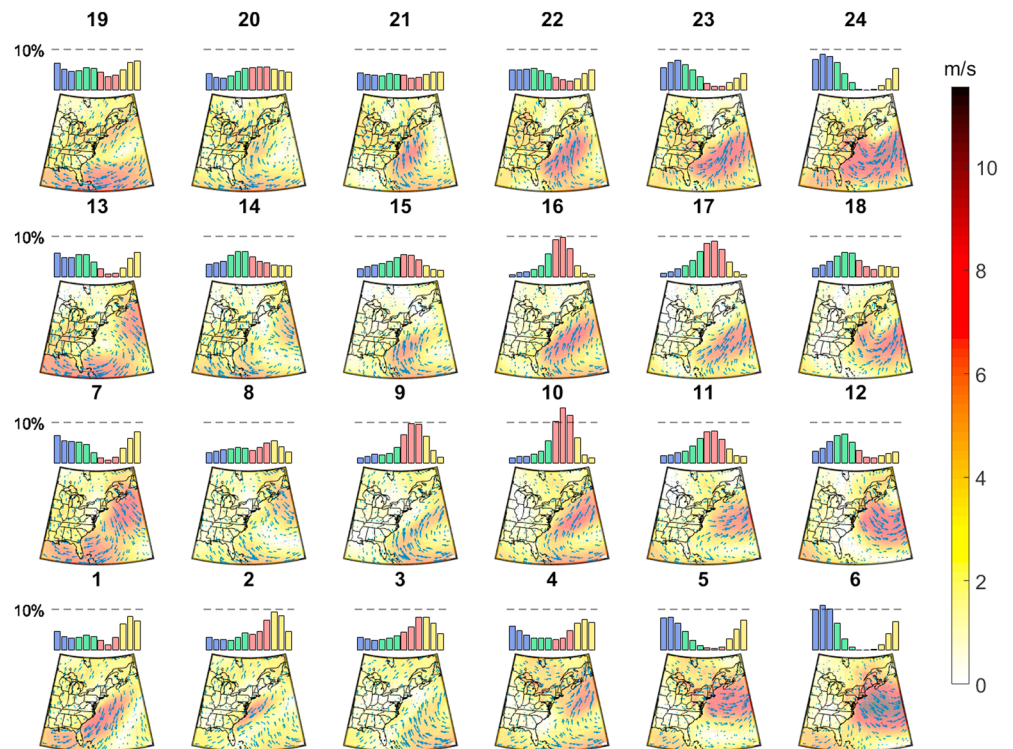


Figure 4. Self-organizing map for the Atlantic domain using 10-m U and V component winds (UVwind). Maps are of mean fields of all days classified into each of the 24 nodes; the colored columns above each map represent the mean monthly frequency of that node over the period of study, December–February (blue), March–May (green), June–August (red), and September–November (yellow).

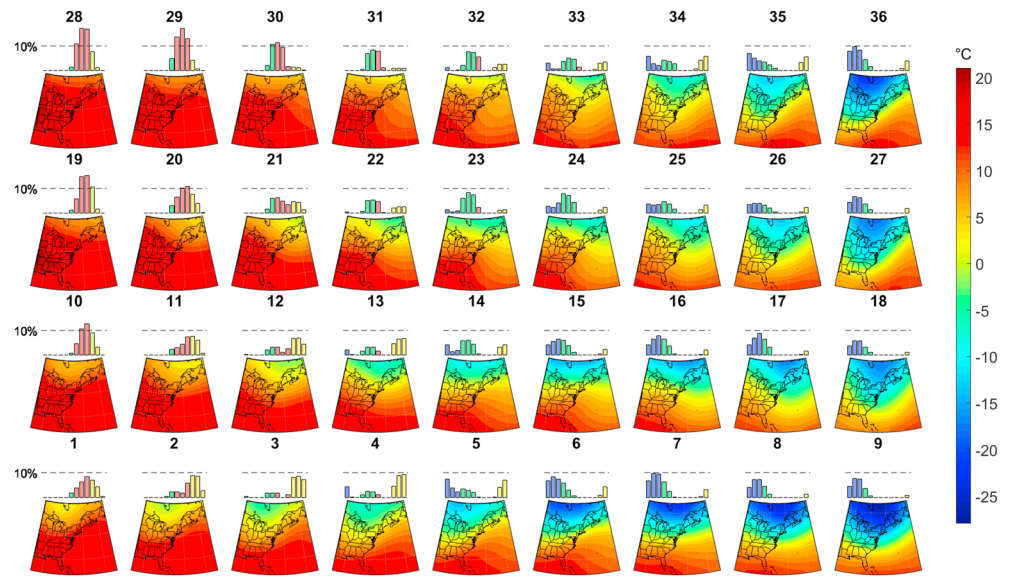


Figure 5. Self-organizing map for the Atlantic domain using 850-mb temperature (850t). Maps are of mean fields of all days classified into each of the 36 nodes; the colored columns above each map represent the mean monthly frequency of that node over the period of study, December–February (blue), March–May (green), June–August (red), and September–November (yellow).

model can reveal the “relative importance of each predictor among all other predictors” (Lee et al., 2017) for the region.

Each NARX model was trained on both open-loop and then closed-loop settings, the former inputting the previous day’s *observed* value of anomalous sea level as an input into the model for the subsequent day’s output, and the latter inputting the previous day’s *modeled* value of anomalous sea level back into the model prediction for the subsequent day. Naturally, the open-loop architecture produces better results (because it uses an actual observed previous value of the predictand in the model itself) and is thus preferable when the aim is to analyze the relationship between predictors and predictand. However, for applications when

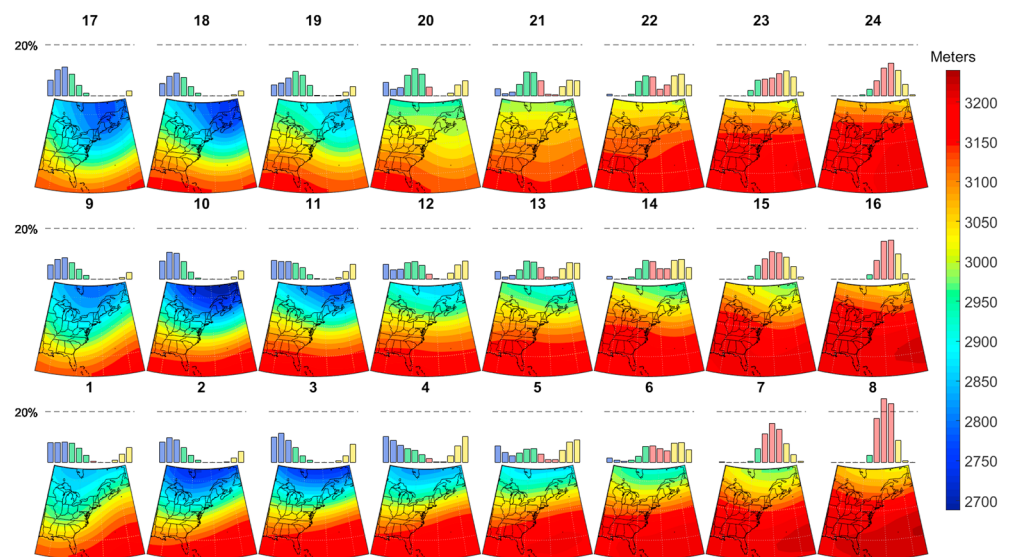


Figure 6. Self-organizing map for the Atlantic domain using 700-mb geopotential height (700z). Maps are of mean fields of all days classified into each of the 24 nodes; the colored columns above each map represent the mean monthly frequency of that node over the period of study, December–February (blue), March–May (green), June–August (red), and September–November (yellow).

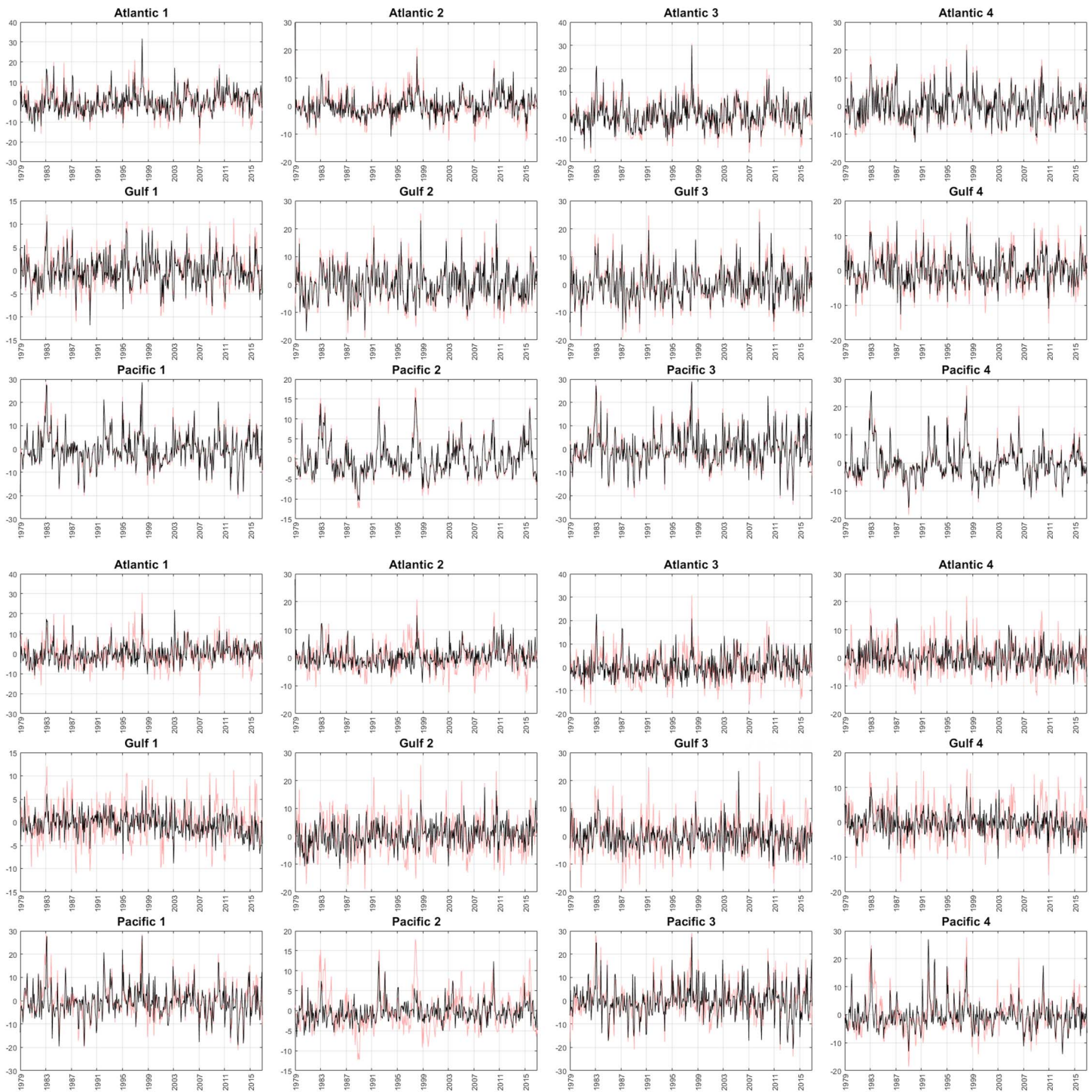


Figure 7. NARX reconstructed (black) and observed (red) monthly time series of anomalous sea level values for the 12 regions for open-loop (top) and closed-loop (bottom) runs in centimeters.

the observed value of the predictand has yet to occur (e.g., forecasting), the closed-loop architecture must be used in order to feed tomorrow's forecast with the estimated/modeled value for today (and so forth in time). Statistics below are presented for both architectures; open-loop results show the ability of the model to learn climate-sea level relationships, while the closed-loop results are more indicative of the potential model skill in future forecasting applications.

Table 1

Spearman's Rho Coefficient of Correlation Between NARX Reconstructed and Observed Daily Sea Level Anomalies for Open-Loop (Top) and Closed-Loop (Bottom) Runs

Month	Atlantic				Gulf				Pacific				AVG
	A1	A2	A3	A4	G1	G2	G3	G4	P1	P2	P3	P4	
	Open-loop results												
Jan	0.73	0.72	0.82	0.79	0.81	0.82	0.85	0.84	0.94	0.89	0.92	0.92	0.84
Feb	0.70	0.76	0.84	0.82	0.84	0.79	0.85	0.85	0.94	0.90	0.92	0.93	0.84
Mar	0.72	0.77	0.83	0.80	0.84	0.81	0.85	0.86	0.93	0.88	0.91	0.92	0.84
Apr	0.74	0.81	0.86	0.84	0.82	0.83	0.86	0.86	0.90	0.85	0.88	0.89	0.84
May	0.69	0.78	0.84	0.83	0.80	0.87	0.89	0.83	0.90	0.91	0.87	0.92	0.84
Jun	0.65	0.74	0.81	0.87	0.78	0.86	0.88	0.80	0.89	0.91	0.87	0.92	0.83
Jul	0.54	0.63	0.76	0.84	0.73	0.88	0.89	0.82	0.87	0.92	0.84	0.90	0.80
Aug	0.58	0.63	0.77	0.84	0.70	0.84	0.84	0.75	0.84	0.93	0.79	0.90	0.78
Sep	0.67	0.73	0.78	0.87	0.83	0.86	0.87	0.81	0.87	0.93	0.83	0.89	0.83
Oct	0.72	0.74	0.83	0.86	0.83	0.88	0.91	0.88	0.89	0.92	0.88	0.90	0.85
Nov	0.73	0.68	0.83	0.82	0.81	0.81	0.87	0.88	0.89	0.90	0.87	0.86	0.83
Dec	0.71	0.70	0.80	0.80	0.83	0.79	0.86	0.85	0.92	0.89	0.90	0.91	0.83
Year	0.68	0.73	0.81	0.83	0.81	0.83	0.87	0.84	0.90	0.90	0.88	0.91	0.83
	Closed-loop results												
Jan	0.69	0.72	0.70	0.57	0.74	0.64	0.73	0.82	0.90	0.57	0.87	0.81	0.73
Feb	0.67	0.72	0.73	0.63	0.74	0.61	0.72	0.83	0.92	0.65	0.91	0.86	0.75
Mar	0.67	0.71	0.70	0.61	0.76	0.63	0.75	0.82	0.89	0.44	0.89	0.76	0.72
Apr	0.71	0.73	0.72	0.64	0.64	0.64	0.76	0.74	0.83	0.24	0.85	0.66	0.68
May	0.63	0.66	0.69	0.55	0.38	0.50	0.60	0.59	0.76	0.42	0.74	0.63	0.60
Jun	0.61	0.63	0.60	0.56	0.42	0.52	0.59	0.43	0.67	0.24	0.74	0.60	0.55
Jul	0.45	0.53	0.44	0.51	0.26	0.58	0.54	0.30	0.54	0.42	0.62	0.50	0.48
Aug	0.51	0.49	0.45	0.42	0.22	0.37	0.38	0.26	0.42	0.34	0.48	0.34	0.39
Sep	0.62	0.60	0.55	0.60	0.46	0.45	0.49	0.48	0.52	0.22	0.65	0.33	0.50
Oct	0.69	0.66	0.68	0.62	0.58	0.61	0.75	0.75	0.72	0.35	0.82	0.52	0.65
Nov	0.75	0.69	0.70	0.62	0.70	0.66	0.77	0.81	0.83	0.38	0.86	0.66	0.70
Dec	0.71	0.71	0.69	0.52	0.73	0.66	0.76	0.83	0.87	0.45	0.89	0.74	0.71
Year	0.64	0.66	0.64	0.56	0.59	0.58	0.66	0.69	0.79	0.40	0.81	0.66	0.64

Note. Colors indicate strength of relationship, with greater relationships in hues of red, and weaker relationships in green.

3. Results and Discussion

3.1. Tidal Gauge Regionalization

The K-means clustering of the tidal gauge station data identified four regions in each of the three domains of the study, for a total of 12 tidal gauge regions (Figure 2). These 12 regions are all spatially cohesive and distinct, with the sole exception of Regions 1 and 3, both along the mid-Atlantic Coast, for which one key delineator is open ocean (Region A3) and bay (A1) gauges.

3.2. SOMs

The SOMs that were created are shown in Figures 3–6 for the Atlantic Domain, and Figures S1–S4 and S5–S8 in the supporting information for the Gulf and Pacific domains, respectively. The SLP SOM (Figure 3) depicts a clear partition of pressure patterns, with the strongest pressure centers occupying three of the four corners. Seasonality can also be readily seen in the frequency of these patterns; for instance, the strong continental high (Node 22) and coastal low/Icelandic low (Nodes 14, 21, and 28) are all winter dominant, while manifestations of the Bermuda/Azores high (e.g., Nodes 12, 19, and 26) are summer dominant. The wind SOM (Figure 4) tends to put fields with stronger winds toward the periphery, and weaker winds in the center, although the cohesiveness of the nodes is more ambiguous than with other variables. Significant off-

Table 2
Median Absolute Error Between Observed Sea Level Anomalies and NARX Modeled Daily Sea Level Anomalies (in Centimeters)

Month	Atlantic				Gulf				Pacific				AVG
	A1	A2	A3	A4	G1	G2	G3	G4	P1	P2	P3	P4	
	Open-loop results												
Jan	8.56	6.38	5.90	4.43	3.78	4.37	3.91	4.43	3.26	1.84	4.43	2.29	4.46
Feb	8.28	5.81	5.73	4.15	3.55	4.30	3.91	4.20	3.31	1.83	4.14	2.56	4.31
Mar	7.41	5.29	5.49	3.55	3.09	4.37	3.70	3.88	3.27	1.76	4.03	2.50	4.03
Apr	6.39	4.12	4.76	3.30	2.74	4.20	3.62	3.26	2.77	1.51	3.37	2.06	3.51
May	5.59	3.16	3.81	2.97	2.23	3.25	2.76	2.91	2.23	1.26	2.89	1.62	2.89
Jun	4.95	2.75	3.62	2.83	1.94	3.06	2.69	2.35	1.97	1.17	2.44	1.60	2.61
Jul	4.40	2.61	3.32	2.78	2.01	2.68	2.41	2.74	1.63	1.00	2.13	1.34	2.42
Aug	4.61	2.84	3.66	3.12	2.21	2.86	3.09	2.75	1.79	1.12	2.27	1.43	2.64
Sep	5.91	2.91	4.72	2.99	2.47	3.88	3.32	2.98	1.88	1.22	2.58	1.48	3.03
Oct	6.43	3.96	4.77	3.21	3.04	3.56	3.00	3.27	2.43	1.41	3.47	1.66	3.35
Nov	7.02	5.09	5.33	3.47	3.55	4.41	3.21	4.04	3.29	1.76	4.78	2.25	4.02
Dec	7.54	5.93	5.90	3.73	3.40	4.82	3.70	4.34	3.65	1.97	5.06	2.56	4.38
Year	6.24	3.90	4.60	3.32	2.73	3.72	3.22	3.32	2.48	1.43	3.26	1.86	3.34
	Closed-loop results												
Jan	9.28	6.51	7.93	6.69	4.69	6.73	5.47	5.18	4.55	3.68	5.57	3.84	5.84
Feb	8.32	6.27	7.78	5.84	4.30	6.49	5.38	4.51	4.08	3.48	4.86	4.06	5.45
Mar	8.49	6.57	8.18	5.40	4.03	6.56	5.66	4.77	4.22	3.64	4.83	4.19	5.55
Apr	7.49	5.25	6.92	5.04	3.95	6.34	4.98	4.68	3.47	3.46	3.99	3.52	4.92
May	6.18	4.17	5.43	4.86	3.87	6.42	5.61	4.50	3.63	3.05	3.95	3.36	4.59
Jun	5.61	3.45	5.22	5.22	3.06	5.29	5.15	3.75	3.56	3.14	3.71	3.43	4.22
Jul	5.05	3.17	5.29	4.89	3.26	4.74	4.84	4.39	3.05	2.60	3.12	2.69	3.93
Aug	4.93	3.50	5.84	5.65	3.22	5.54	5.44	4.17	3.22	2.64	3.32	3.34	4.23
Sep	6.41	3.68	7.01	5.64	4.43	7.89	6.18	4.56	3.50	3.74	4.09	3.63	5.06
Oct	7.22	4.92	6.89	5.19	4.57	6.19	5.13	4.58	3.89	4.13	4.49	3.75	5.08
Nov	6.65	5.23	6.99	5.34	4.53	6.62	4.96	5.11	4.66	3.82	5.50	3.74	5.26
Dec	8.30	6.23	7.54	6.63	4.69	6.36	5.40	5.27	5.24	4.01	5.73	4.62	5.83
Year	6.75	4.66	6.63	5.50	3.99	6.20	5.35	4.57	3.83	3.39	4.29	3.61	4.90

Note. Colors indicate strength of relationship, with greater relationships in hues of red, and weaker relationships in green.

shore flow can be seen in some winter-dominant patterns (e.g., Nodes 6, 7, and 24), with southerly flow common across many of the summer-dominant middle nodes, displaying the wind fields associated with the Bermuda/Azores high.

In contrast to the above, the SOMs for 850-mb temperature (T850; Figure 5) and 700-mb geopotential height (700Z; Figure 6) are arranged primarily in a reflection of seasonality, as these two variables have strong inter-seasonal variability. T850 nodes thus reflect variations in the thermal gradient in each season, with generally lesser gradients on top, and greater gradients on bottom, of an array where summer patterns are on the left and winter on right. 700Z nodes are arranged in a similar partition, with season itself shifting from left to right, and magnitude of height gradient changing from top to bottom.

3.3. Modeled Sea Level Anomalies and Validation

The NARX-reconstructed time series of anomalous sea levels are shown in Figure 7 (shown with monthly values to improve readability) with daily correlation statistics in Table 1. The reconstructed monthly time series show the ability of the APs and their PCs to be used collectively to project sea level anomalies. Many monthly peaks are well simulated, most notably the increased sea levels across all regions nearly universally during the 1997–1998 El Niño, and the 1982–1983 El Niño in the Pacific regions, along with extreme low sea levels in the Pacific region during the 1988–1989 La Niña. The model also simulates well the 2009–

Table 3
Hit Rates for the 95th Percentile of Daily Sea Level Anomalies (i.e., the Percentage of Actual Sea Level Anomalies in the Top 5th Percentile That Are Also Identified as Such in the NARX Model)

Month	Atlantic				Gulf				Pacific				AVG	
	A1	A2	A3	A4	G1	G2	G3	G4	P1	P2	P3	P4		
	OPEN-LOOP RESULTS													
Jan	45%	50%	53%	62%	50%	55%	45%	45%	69%	74%	60%	67%	56%	
Feb	48%	52%	52%	63%	50%	54%	46%	43%	72%	78%	65%	74%	58%	
Mar	56%	47%	51%	61%	54%	53%	64%	59%	71%	69%	64%	68%	60%	
Apr	51%	54%	49%	54%	46%	56%	65%	61%	77%	72%	67%	82%	61%	
May	47%	56%	56%	49%	58%	58%	73%	64%	69%	64%	56%	69%	60%	
Jun	46%	44%	53%	65%	56%	61%	75%	63%	67%	70%	53%	61%	59%	
Jul	32%	42%	37%	58%	47%	61%	64%	54%	53%	76%	47%	66%	53%	
Aug	47%	36%	53%	63%	56%	63%	59%	63%	64%	75%	58%	73%	59%	
Sep	46%	39%	53%	61%	53%	64%	61%	49%	72%	77%	65%	70%	59%	
Oct	54%	46%	59%	64%	61%	55%	75%	56%	64%	80%	66%	66%	62%	
Nov	56%	44%	63%	61%	40%	54%	51%	49%	67%	84%	61%	72%	59%	
Dec	53%	39%	64%	75%	56%	54%	66%	58%	54%	66%	56%	58%	58%	
Year	51%	50%	58%	64%	55%	58%	61%	56%	75%	75%	67%	75%	62%	
	CLOSED-LOOP RESULTS													
Jan	34%	43%	47%	47%	40%	26%	33%	43%	59%	21%	45%	50%	41%	
Feb	43%	46%	43%	48%	39%	35%	35%	44%	69%	50%	59%	56%	47%	
Mar	41%	39%	41%	49%	51%	32%	42%	61%	61%	51%	63%	53%	49%	
Apr	44%	46%	40%	49%	32%	26%	46%	44%	74%	30%	53%	63%	45%	
May	41%	39%	44%	36%	29%	22%	20%	32%	61%	8%	51%	34%	35%	
Jun	39%	44%	32%	33%	37%	18%	36%	28%	47%	0%	54%	9%	31%	
Jul	25%	36%	17%	20%	24%	33%	27%	29%	34%	5%	36%	19%	25%	
Aug	25%	32%	34%	24%	36%	32%	24%	27%	25%	10%	44%	10%	27%	
Sep	32%	23%	35%	25%	37%	31%	47%	37%	28%	12%	42%	14%	30%	
Oct	42%	44%	39%	47%	42%	31%	41%	46%	66%	31%	66%	31%	44%	
Nov	49%	39%	39%	40%	28%	21%	33%	40%	53%	28%	53%	53%	40%	
Dec	51%	34%	58%	58%	32%	34%	29%	39%	51%	20%	44%	56%	42%	
Year	43%	46%	42%	41%	41%	30%	37%	45%	67%	29%	62%	57%	45%	

Note. Yellow boxes indicate hit rates below 5%.

2010 increase in sea level rise along the Atlantic Coast as observed by Goddard et al. (2015). As coastal vulnerability in the Pacific region has been tied to El Niño events (Barnard et al., 2015), the ability of the NARX to simulate these anomalies is promising. Within these simulations, both aggregated to the monthly level (Figure 7) and at the daily level (Table 1), it is clear that the open-loop run, in which previously observed data can be used to model subsequent data, outperforms the closed-loop run, particularly with extreme events, suggesting that while there is a strong connection between anomalous sea levels and APs, the model is partly dependent upon autocorrelation of the sea level time series.

The NARX models also show considerable variability in skill across space and time. Across the Pacific regions, the greatest overall correlations are observed, with the weakest across the Atlantic regions. This general pattern is similar to other nuisance flood modeling work (e.g., Vandenberg-Rodes et al., 2016). Weaker correlations within each domain are seen in the regions which contain substantive bays, such as A1 (Chesapeake and Delaware Bays), the region with the weakest overall correlation using open-loop, and P3 (Puget Sound). Overall, skill is greater during the cold season than during the warm season, particularly in the northern regions of both Atlantic and Pacific Coasts. As expected, the closed-loop results do not perform as well as the open-loop results at all regions, though the magnitude of difference varies widely. Using closed-loop, summer correlations decrease the most substantially across all regions, indicative of the decreased variability from AP to AP over the summer, in comparison with other regions, and thus the

Table 4
Relative Importance of Each Predictor Variable on NARX Models in Each Region

	Atlantic				Gulf				Pacific				AVG
	A1	A2	A3	A4	G1	G2	G3	G4	P1	P2	P3	P4	
SLP	6%	6%	6%	7%	6%	6%	5%	6%	7%	7%	7%	7%	6%
850T	7%	8%	7%	7%	8%	10%	8%	9%	8%	8%	8%	8%	8%
WIND	7%	7%	7%	7%	8%	8%	7%	8%	7%	8%	8%	8%	7%
700Z	7%	7%	7%	7%	7%	7%	7%	8%	7%	8%	8%	8%	7%
PCs (SLP)	17%	16%	17%	17%	14%	15%	13%	14%	13%	15%	14%	13%	15%
PCs (800T)	13%	12%	13%	14%	13%	12%	12%	13%	10%	13%	11%	13%	12%
PCs (WIND)	16%	16%	16%	16%	14%	16%	14%	14%	13%	14%	13%	14%	15%
PCs (700Z)	14%	14%	14%	13%	14%	14%	12%	13%	12%	14%	13%	14%	14%
Season	4%	4%	4%	5%	4%	3%	10%	5%	6%	7%	5%	4%	5%
Trend	9%	8%	9%	7%	11%	8%	11%	11%	17%	7%	13%	12%	10%

Note. Colors indicate strength of relationship, with greater relationships in hues of red, and weaker relationships in green. PC = principal component; SLP = sea level pressure.

lesser utility broader-scale atmospheric conditions would have in predicting anomalous sea level in future forecasting applications. MDAEs of the NARX models show average daily anomalous sea level errors of less than 4 cm with open-loop models and less than 5 cm with closed-loop models when averaged across all months and regions, with seasonal and geographic variability largely mimicking the Spearman correlation results (Table 2).

Aside from these correlations that cover the entire range of sea level anomalies, we also examined the ability of the NARX models to simulate the very highest daily sea level anomalies, and thus the occasions when flooding is most likely (Tables 3 and A1). Variability in the hit rates is similar to those of the Spearman correlations, with generally improved skill during the cold season—with a more pronounced seasonality to hit rates on closed-loop (i.e., hit rates on open-loop do not decline nearly as much in summer). Skill was generally greatest in Pacific Regions P1, P2, and P4, where even in the closed-loop run over 50% of high-water events were correctly simulated.

Input variables ranged in performance depending on the region, with the retained PCs (those with eigenvalues > 1) for circulation pattern development generally playing the most important role in the models (Table 4). The APs accounted for anywhere between 5% to 10% of the change in model performance, with the 850T SOM weighing the heaviest. The two time-based variables, seasonality (5%) and trend (10%), played varying roles, with seasonality becoming more important near the mouth of the Mississippi River and trend being most important along the coast of Northern California and Oregon.

4. Conclusions

Projections of nuisance floods in the coming decades suggest that their frequency will reflect the sharp upward in trend observed in the past decade (Sweet et al., 2018; Vandenberg-Rodes et al., 2016). With this in mind, it is imperative to prepare coastal communities not only in terms of planning for their long-term increase in frequency but also in the short-term forecasting of their likelihood in the near term. In our research, we have shown that the use of four atmospheric fields on a subcontinental scale—sea level pressure, 10-m winds, 700-mb geopotential height, and 850-mb temperature—can be successfully used to predict anomalous sea level values, as well as the occurrence of extreme sea level anomalies. Modeling ability varies spatially and temporally across the United States, with better performance in winter than summer, and along the Pacific Coast.

That fields of atmospheric variables can be used to predict anomalous sea level values along coastlines is beneficial, as it allows an assessment of weather (or climate) forecasting models to simulate the fields of these variables. Next, we plan to assess weather forecasting model ability to simulate the APs derived in this research, with the hypothesis that model ability to replicate these patterns can yield prospective nuisance flood forecasts in the subseasonal to seasonal timeframe.

Data Availability

The input data for this research are all publicly available. The NARR data used for atmospheric modeling can be obtained from the website (<https://www.ncdc.noaa.gov/data-access/model-data/model-datasets/north-american-regional-reanalysis-narr>). The NOAA COOPS tidal data can be obtained from the <https://tidesandcurrents.noaa.gov> website. The data explicitly generated in this research (region-wide daily sea level anomalies; NARX-modeled daily sea level anomalies; daily SOM classifications) are available on Mendeley Data (<https://data.mendeley.com/datasets/r59jdbwvwmn/1>).

Acknowledgments

Funding for this project has been provided by the Climate Program Office of NOAA, Federal Award NA17OAR4310113.

References

- Barnard, P. L., Short, A. D., Harley, M. D., Splinter, K. D., Vitousek, S., Turner, I. L., et al. (2015). Coastal vulnerability across the Pacific dominated by El Niño/Southern oscillation. *Nature Geoscience*, *8*(10), 801–807. <https://doi.org/10.1038/ngeo2539>
- Beale, M. H., Hagan, M. T., & Demuth, H. B. (2010). *Neural network toolbox user's guide, R2014a. White Paper*. Natick, MA (USA): The Mathworks Inc.
- Beck, C., Philipp, A., & Streicher, F. (2013). The effect of domain size on the relationship between circulation type classifications and surface climate. *International Journal of Climatology*, *36*, 2692–2709.
- Carrere, L., & Lyard, F. (2003). Modeling the barotropic response of the global ocean to atmospheric wind and pressure forcing—comparisons with observations. *Geophysical Research Letters*, *30*(6), 1275. <https://doi.org/10.1029/2002GL016473>
- Cassano, E. N., Lynch, A. H., Cassano, J. J., & Koslow, M. R. (2006). Classification of synoptic patterns in the western Arctic associated with extreme events at Barrow, Alaska, USA. *Climate Research*, *30*, 83–97. <https://doi.org/10.3354/cr030083>
- Cazenave, A., Dieng, H. B., Meyssignac, B., von Schuckmann, K., Decharme, B., & Berthier, E. (2014). The rate of sea-level rise. *Nature Climate Change*, *4*(5), 358–361. <https://doi.org/10.1038/nclimate2159>
- Church, J. A., & White, N. J. (2011). Sea-level rise from the late 19th to the early 21st century. *Survey of Geophysics*, *32*(4-5), 585–602. <https://doi.org/10.1007/s10712-011-9119-1>
- Colle, B. A., Rojowsky, K., & Buonaito, F. (2010). New York City storm surges: Climatology and an analysis of the wind and cyclone evolution. *Journal of Applied Meteorology and Climatology*, *49*(1), 85–100. <https://doi.org/10.1175/2009JAMC2189.1>
- Davies, D. L., & Bouldin, D. W. (1979). A cluster separation measure. *IEEE Transactions on Pattern Analysis and Machine Intelligence*, *PAMI-1*(2), 224–227. <https://doi.org/10.1109/TPAMI.1979.4766909>
- Diaconescu, E. (2008). The use of NARX neural networks to predict chaotic time series. *Wseas Transactions on Computer Research*, *3*, 182–191.
- Goddard, P. B., Yin, J., Griffies, S. M., & Zhang, S. (2015). An extreme event of sea-level rise along the Northeast coast of North America in 2009–2010. *Nature Communications*, *6*(1), 6346. <https://doi.org/10.1038/ncomms7346>
- Hamlington, B. D., Leben, R. R., Kim, K. Y., Nerem, R. S., Atkinson, L. P., & Thompson, P. R. (2015). The effect of the El Niño-Southern Oscillation on US regional and coastal sea level. *Journal of Geophysical Research: Oceans*, *120*, 3970–3986. <https://doi.org/10.1002/2014JC010602>
- Hewitson, B. C., & Crane, R. G. (2002). Self-organizing maps: Applications to synoptic climatology. *Climate Research*, *22*, 13–26. <https://doi.org/10.3354/cr022013>
- Jevrejeva, S., Moore, J. C., & Grinsted, A. (2003). Influence of the Arctic Oscillation and El Niño-Southern Oscillation (ENSO) on ice conditions in the Baltic Sea: The wavelet approach. *Journal of Geophysical Research*, *108*(D21), 4677. <https://doi.org/10.1029/2003JD003417>
- Landerer, F. W., & Volkov, D. L. (2013). The anatomy of recent large sea level fluctuations in the Mediterranean Sea. *Geophysical Research Letters*, *40*, 553–557. <https://doi.org/10.1002/grl.50140>
- Lee, C. C. (2017). Reanalysing the impacts of atmospheric teleconnections on cold-season weather using multivariate surface weather types and self-organizing maps. *International Journal of Climatology*, *37*(9), 3714–3730. <https://doi.org/10.1002/joc.4950>
- Lee, C. C., & Sheridan, S. C. (2015). Synoptic climatology: An overview. In *Reference Module in Earth Systems and Environmental Sciences*. Amsterdam: Elsevier. <https://doi.org/10.1016/B978-0-12-409548-9.09421-5>
- Lee, C. C., Sheridan, S. C., Barnes, B. B., Hu, C., Pirhalla, D. E., Ransibrahmanakul, V., & Shein, K. (2017). The development of a non-linear auto-regressive model with exogenous input (NARX) to model climate-water clarity relationships: reconstructing an historical water clarity index for the coastal waters of the southeastern US. *Theoretical and Applied Climatology*, *130*(1-2), 557–569. <https://doi.org/10.1007/s00704-016-1906-7>
- Mesinger, F., DiMego, G., Kalnay, E., Mitchell, K., Shafran, P. C., Ebisuzaki, W., et al. (2006). North American Regional Reanalysis. *Bulletin of the American Meteorological Society*, *87*(3), 343–360. <https://doi.org/10.1175/BAMS-87-3-343>
- National Oceanic and Atmospheric Administration (2013). Service assessment: Hurricane/Post-Tropical Cyclone Sandy—October 22-29, 2012. 46pp.
- Neal, R., Dankers, R., Saulter, A., Lane, A., Millard, J., Robbins, G., & Price, D. (2018). Use of probabilistic medium-to long-range weather-pattern forecasts for identifying periods with an increased likelihood of coastal flooding around the UK. *Meteorological Applications*, *25*(4), 534–547. <https://doi.org/10.1002/met.1719>
- Philipp, A., Beck, C., Huth, R., & Jacobeit, J. (2014). Development and comparison of circulation type classifications using the COST 733 dataset and software. *International Journal of Climatology*, *36*, 2673–2691.
- Pieuch, C. G., & Ponte, R. M. (2011). Mechanisms of interannual steric sea level variability. *Geophysical Research Letters*, *38*, L15605. <https://doi.org/10.1029/2011GL048440>
- Pirhalla, D. E., Sheridan, S. C., Ransi, V., & Lee, C. C. (2015). Assessing cold-snap and mortality events in South Florida coastal ecosystems: Development of a biological cold stress index using satellite SST and weather pattern forcing. *Estuaries and Coasts*, *38*(6), 2310–2322. <https://doi.org/10.1007/s12237-014-9918-y>
- Schoof, J. T. (2013). Statistical downscaling in climatology. *Geography Compass*, *7*(4), 249–265. <https://doi.org/10.1111/gec3.12036>
- Sheridan, S. C., & Lee, C. C. (2011). The self-organizing map in synoptic climatological research. *Progress in Physical Geography*, *35*(1), 109–119. <https://doi.org/10.1177/0309133310397582>
- Sheridan, S. C., Lee, C. C., Pirhalla, D. E., & Ransibrahmanakul, V. (2017). Atmospheric drivers of sea-level fluctuations and nuisance floods along the mid-Atlantic coast of the USA. *Regional Environmental Change*, *17*(6), 1853–1861. <https://doi.org/10.1007/s10113-017-1156-y>

- Sweet, W. V., Dusek, G. P., Obeysekera, J., Marra, J. J. (2018). Patterns and projections of high tide flooding along the US coastline using a common impact threshold. U.S. Department of Commerce, National Oceanic and Atmospheric Administration, National Ocean Service, Center for Operational Oceanographic Products and Services, 56 pp.
- Sweet, W. V., Zervas, C., Gill, S. (2009). Elevated east coast sea level anomaly: June–July 2009, NOAA Tech. Rep. No. NOS CO-OPS 051, NOAA National Ocean Service, Silver Spring, MD, 40 pp.
- Thompson, P. R., Mitchum, G. T., Vonesch, C., & Li, J. (2013). Variability of winter storminess in the eastern United States during the twentieth century from tide gauges. *Journal of Climate*, *26*(23), 9713–9726. <https://doi.org/10.1175/JCLI-D-12-00561.1>
- Vandenberg-Rodes, A., Mofakhari, H. R., AghaKouchak, A., Shahbaba, B., Sanders, B. F., & Matthew, R. A. (2016). Projecting nuisance flooding in a warming climate using generalized linear models and Gaussian processes. *Journal of Geophysical Research: Oceans*, *121*, 8008–8020. <https://doi.org/10.1002/2016JC012084>
- Wetterhall, F., Bárdossy, A., Chen, D., Halldin, S., & Xu, C. Y. (2009). Statistical downscaling of daily precipitation over Sweden using GCM output. *Theoretical and Applied Climatology*, *96*(1-2), 95–103. <https://doi.org/10.1007/s00704-008-0038-0>
- Wöppelmann, G., & Marcos, M. (2016). Vertical land motion as a key to understanding sea level change and variability. *Reviews of Geophysics*, *54*, 64–92. <https://doi.org/10.1002/2015RG000502>
- Wunsch, C., & Stammer, D. (1997). Atmospheric loading and the oceanic “inverted barometer” effect. *Reviews of Geophysics*, *35*(1), 79–107. <https://doi.org/10.1029/96RG03037>
- Yarnal, B. (1993). *Synoptic climatology in environmental analysis: A primer*. London: Belhaven press.